



Evaluation of the geometry for remote river rating in hydrodynamic environments.

Hubert T. Samboko¹, Sten Schurer¹, Hubert H.G. Savenije¹, Hodson Makurira², Kawawa Banda³, Hessel Winsemius^{1, 4, 5}

5 ¹Department of Water Resources, Faculty of Civil Engineering and Geosciences, Delft University of Technology, Stevinweg 1, 2628 CN, Delft, Netherlands

²Department of Construction and Civil Engineering, University of Zimbabwe, Box MP 167, Mt. Pleasant, Harare, Zimbabwe

³Department of Geology, Integrated Water Resources Management Centre, University of Zambia, Great East Road Campus, P.O. Box 32379, Lusaka, Zambia

10 ⁴Deltares, Delft, the Netherlands

⁵Rainbow Sensing, The Hague, the Netherlands

Correspondence to: Hubert T. Samboko (hsamboko@gmail.com)

Abstract. Rapid modern technological advancements have led to significant improvements in river monitoring using Unmanned Aerial vehicles (UAVs). These UAVs allow for the collection of flow geometry data in environments that are difficult to access. Hydraulic models may be constructed from these data, which in turn can be used for various applications such as water management, forecasting, early warning and disaster preparedness by responsible water authorities, and construction of river rating curves. We hypothesize that the reconstruction combined with Real Time Kinematic Global Navigation Satellite System (RTK GNSS) equipment leads to accurate geometries particularly fit for hydraulic understanding and simulation models. This study sought to (1) compare open source and commercial photogrammetry packages to verify if water authorities with low resource availability have the option to utilise these without significant compromise on accuracy; (2) assess the impact of variations in the number of Ground Control Points (GCPs) and the distribution of the GCP markers on the quality of Digital Elevation Models (DEMs), with a particular emphasis on characteristics that impact on hydraulics; and (3) investigate the impact of variations in DEMs on flow estimations based on the number of GCPs used. We tested our approach over a section of the Luangwa River in Zambia. We compare performance of two different photogrammetry software packages, one being open-source and one commercial; then compare for one chosen package the performance with different GCP numbers and distributions, and finally, emphasize on the reconstruction of hydraulically important parameters. The first investigation (1) utilises the root mean square error (RMSE) method to determine if open source software performs as well as commercial software. The second task (2) aimed to assess the optimal GCP number and distribution; we generated 10 UAV based elevation models under varying GCP distribution conditions using OpenDroneMap (ODM) software. To benchmark the different DEM reconstructions we assessed the Mean Absolute Error of the elevation using the GCPs that were left out of the reconstruction. Finally (3), in order to investigate the impact of variations in DEMs on flow estimations we performed a comparison of the hydraulic conveyance across each reconstruction, as well as a comparison of the hydraulic slope against an independent estimate using an in-situ RTK GNSS tie line. Results indicate that the open-source software photogrammetry



35 package is capable of producing results that are comparable to commercially available options. We determined that GCPs are
essential for vertical accuracy, but also that an increase in the number of GCPs above a limited amount of 5 only moderately
increases the accuracy of results, provided the GCPs are well spaced both in horizontal and vertical dimension. Furthermore,
insignificant differences in hydraulic geometries among the various cross sections are observed, corroborating the fact that a
limited well-spaced set of GCPs is enough to establish a hydraulically sound reconstruction. This is important so that future
studies do not invest in procedures that may be costly, but may not contribute significantly to the improvement of desired
40 results. The hydraulic slope was shown to be prone to errors caused by lens distortion. These errors are too large to enable use
in a hydraulic model setup. We therefore recommend to combine photogrammetry results with a RTK GNSS tie line when
reconstructions are to be used for hydraulic model setup.

Key Words: Unmanned Aerial Vehicle, Digital Elevation Model, Ground Control Point, Conveyance

1 Introduction

45 Traditionally, flow measurements are performed through the use of current meters. A combination of measured depth and
velocities across a profile can be integrated to calculate the total discharge. In order to attain continuous discharge data, river
stage is recorded and plotted against corresponding discharge measurements to produce rating curves (Hersch, 2009; Mosley
and McKerchar, 1993). Ideally, discharge measurements are carried out over a wide range of river stages. The low and medium
river stages are usually relatively easy to record whereas the high river stages are difficult as they are associated with dangerous
50 conditions such as floods and inaccessible terrains. Peaks are also easy to miss, as deployment of personnel and materials takes
time. Due to these difficulties, high stage discharge measurements are usually extrapolated from the rating curve. On the other
hand, there is the risk of high variability in low flow measurements as a result of changing bed configurations, particularly in
sand rivers which change every season. Measurement are usually taken at one particular point frequently despite physical
changes in the profile. These problems lead to high levels of uncertainty in discharge estimates which makes it difficult for
55 water authorities to understand stream generation especially during high flows when management is mostly required (Petersen-
Øverleir et al., 2009). Another limitation is the time validity of the measurements which strongly depends on factors such as
river bed degradation, river course changes after floods and overflow or ponding in areas adjoining the stream channel
(Hersch, 2009; Rantz and Others, 1982).

Using a hydraulic modelling strategy has become an alternative for discharge estimation (Mansanarez et al., 2019). Physically
60 based river rating is based on capturing geometry in a power law expression. The physically based river rating makes use of
the fact that river flow is a function of river slope, river-bed roughness and channel geometry. In this instance discharge
measurements of flow require information about the geometry of the channel in question (Costa et al., 2000). One of the most
commonly used equations is Manning's formula which is based on steady and uniform flow (Chow, 1959).



The Manning equation can be rewritten as the power law function Eq. (1):

$$Q = n^{-1}\sqrt{i}(AR^{2/3}), \quad (1)$$

65 where Q is discharge [m^3/s], n the Manning's roughness coefficient, i is the bottom slope [-], A is the cross-sectional area [m^2] and R the hydraulic radius [m], [$\text{s m}^{-1/3}$]

In this equation; the first part ($n^{-1}\sqrt{i}$) depends on the bottom slope and channel roughness, the second part ($AR^{2/3}$), depends on the cross-sectional geometry. We refer to the A and R collectively as "hydraulic geometry" and $AR^{2/3}$ as the "conveyance".

70 Geometry is a critical input in the production of rating curves (Zheng et al., 2018). Advancements in technology have allowed for a wide range of options for the establishment of geometry. These methods include survey equipment (levels, theodolites, Differential GNSS), Ground Penetrating Radar, sensors mounted on satellites, aeroplanes, kites, unmanned aerial vehicles (UAV), hot air balloons (Feurer et al., 2008; Salamí et al., 2014). In general, manned aircraft which carry cameras are much more costly than other forms of image data collection (Yang et al., 2006). A low-cost means of collecting geometry is through systematic capturing of images from one or multiple cameras mounted on an unmanned aerial vehicle (UAV). Advancements
75 in technologies have resulted in the ability of surveyors to collect very high-resolution geometrical data in difficult to access places (Samboko et al., 2019).

The advantages of using UAVs are, (i) the portability of UAVs; ii) the option to self-design and modify integrated sensors; (iii) the availability of open source and user-friendly data processing software; (iv) the collection of data in difficult to access terrains and; (v) the relatively low-cost of basic UAVs (Gindraux et al., 2017). UAVs, which operate at low altitudes, have a
80 much higher spatial resolution than satellites and are not limited in temporal resolution. Satellites with high spatial resolution usually have long return periods. Only a very limited amount of studies so far have used UAVs to collect data for hydraulic model purposes. A study was conducted by Mazzoleni (2020) on the potential for using UAV derived topography for hydraulic modelling. The study concluded that these topographies extracted from UAVs presented results comparable to LIDAR and RTK GNSS-based topographies. However, it did not accurately measure the permanently wetted bathymetry of the river.
85 Rather, the study mechanically filtered out the river which brought about some uncertainty. A similar study which investigated the impact of the number of ground control points on flood risk model performance concluded that UAVs could successfully be used for data collection as long as a minimum number of control points were utilised (Coveney and Roberts, 2017). Similar to the previous study, there was no combination of dry and wet land to produce the topography which is the situation in most areas of interest by water authorities. In addition, the processing was conducted using commercially available software



90 packages which may be inhibitive to low budget water resource authorities. The accuracy of geometry is important in that it
can significantly affect the estimated discharge if incorrectly processed. The factors affecting the output can be divided into
three groups; (i) pre-flight (flight application, GCP number), (ii) flight settings (camera angle, direction, velocity, altitude,
light intensity, wind speed, overlap) and (iii) post-flight processing (processing software, GCP combination). There has been
some attempt to review UAV acquisition systems, orientation and regulation (Colomina and Molina, 2014). The application
95 was however limited to the instruments used, i.e. it did not assess the impact of using UAVs for data acquisition in
hydrodynamic environments.

The process of photogrammetry requires software which is usually available at a cost beyond the reach of most researchers
and other interested parties. Some of the more common software packages are (commercial) Pix4D, Agisoft meta-soft and
(non-commercial and open-source) OpenDroneMap (ODM). Several researchers have made some comparisons between the
100 commercially available software (Alidoost and Arefi, 2017; Grussenmeyer and Khalil, 2008; Probst et al., 2018). ODM is an
open-source software which can be used to generate digital elevation models and other photogrammetry results. A comparison
focusing on the processing time was conducted by Zečević (2017), which concluded that cloud-based solutions such as
DroneMapper could produce high-quality elevation models at shorter time spans.

Hydraulic geometry is an important factor that significantly affects the accuracy of discharge estimations in hydraulic models
and is therefore critical for estimating how much water can be conveyed within the channel capacity, and to estimate flow as
105 a function of water levels. A number of factors impact the quality of geometrical elevation models produced through UAV
based photogrammetry. The primary factors are the number of ground control points and the distribution of these marker points
(Awasthi et al., 2019). There exists minimal research on how these factors can be adjusted to improve the quality of elevation
models in hydrodynamic environments and when applied for the ultimate purposes of discharge estimation. Furthermore,
earlier contributions have not put the focus on the ability to reproduce hydraulic geometry characteristics and have not focused
110 on the entire bathymetry (including the permanently wet river bed section). Hence, this paper investigates if low-cost methods
for data collection and processing, i.e. a combination of precise bathymetry points with low-cost RTK, and UAV
photogrammetry, can be used to provide satisfactory quality elevation models for hydraulic models, quantified in hydraulic
geometry characteristics. We focus on low-cost data collection and open-source processing methods. We tested the methods
115 on the Luangwa River in Zambia.

This paper is organised as follows: section 2 describes the methodology and gives a brief outline of what materials were used
in the study. In Section 2.1 describe the study area (Luangwa Basin). Furthermore, the methodology section outlines how flow
estimation was determined and software packages were compared. Furthermore, Section 3 presents results and a discussion of
the results. We conclude with section 4 which presents a conclusion and recommendation for future studies.



120 **2 Materials and Methods**

This section first describes the data collection procedures, including flight plan, collection of ground control point's, dry and wet bathymetry. Then it describes which experiments are conducted to investigate our research questions. We investigate the following research questions and determine whether the said factors have a significant effect on the accuracy of results. These are:

- 125 1. Can the freely available (Open Source) ODM software package produce results that are comparable to commercial packages such as Agisoft Metashape?
2. What is the optimal GCP number and GCP distribution necessary to reconstruct accurate elevation models?
3. What impact does utilising elevation models, reconstructed based on different GCP numbers have on flow estimations?

2.1 Study site

- 130 The study was conducted along the Luangwa River, South of the Luangwa Bridge. The Basin has a catchment area of approximately 160,000 km². The Luangwa River originates in the Mafinga Hills in the North-Eastern part of Zambia and is approximately 850 km in length, flowing in South-Western direction. The river drains into the Zambezi River, shaping a broad valley along its course. The river has naturally created a valley, which is well-known for its abundant wildlife and relatively pristine surroundings (WARMA, 2016). The study area is shown on *Figure 1*.

135

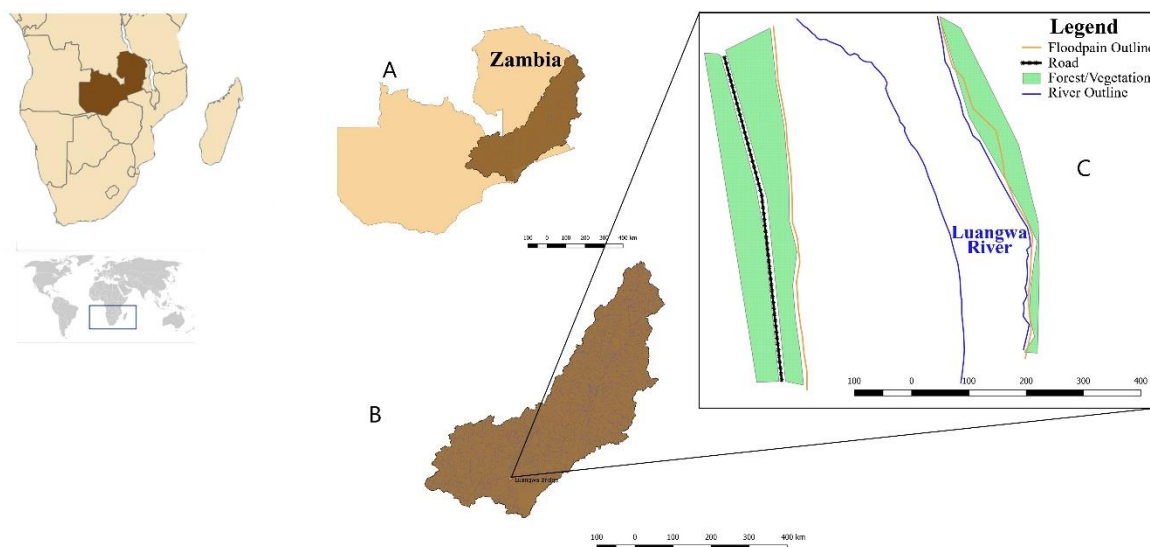


Figure 1 Study area map in Zambia

The data collection was conducted in the late stages of the dry season (December, 2019) to maximise the visible floodplain.

2.2 Data acquisition

140 2.2.1 Flight Plan

GCPs were recorded using RTK GNSS equipment on a 1 km long floodplain. Flights were conducted at two different heights (90m and 100m) at a constant speed, 10^0 camera angle, direction (i.e. parallel or perpendicular to river) and image overlap (80%). The UAV used is a DJI Phantom 4 Advance with a 12 Megapixel FC330 RGB camera. A flight planning android application called Pix4D Capture was used to control the autonomous flights. This application was chosen due to its capability to tilt the camera forward during the image capturing process. Different GCP combinations and variations were tested, including the use of different flight paths. This was done to avoid the so-called “doming effect” (also known as “bowling effect”) i.e. distortion of the reconstruction due to unfortunate acquisition conditions or unreliable modeling of radial lens distortions (Magri and Toldo, 2017). It is important to have only one variable with all other factors remaining constant to allow for comparability. Some guidelines for avoiding the doming effect have been outlined (James and Robson, 2014).

150 2.2.2 Dry river bathymetry

In order to refine the camera calibration parameters and to optimise the geometry of the output, GCPs have to be used. The dry bathymetry data collection can be divided into two procedures; placing the GCPs on the ground and collecting the images. A total of 17 GCP markers were placed on the floodplain, with some being closer to the road, others more in the middle of the dry floodplain and the last closer to the water line. *Figure 2* shows the location of the GCPs in relation to the floodplain. An



155 effort was made to make sure all elevation variations were covered by the placement of GCPs. The markers were 40 cm by 40
cm in dimension and had an alternating black/white colour. The markers were placed on one side of the floodplain because the
other side was steep and covered with dense vegetation. An Arduino simpleRTK2B GNSS, equipped with a u-blox ZED-F9P
dual frequency GNSS receiver was then used to record the marker points. The simpleRTK2B set is a low-cost GNSS with
<1cm level precision with base-rover and <1cm level precision with NTRIP corrections. *Figure 3 (a)* shows the SimpleRTK2B
160 Base and Rover which was used to measure marker points. *Figure 3 (b)* shows the simpleRTK2B setup onsite.

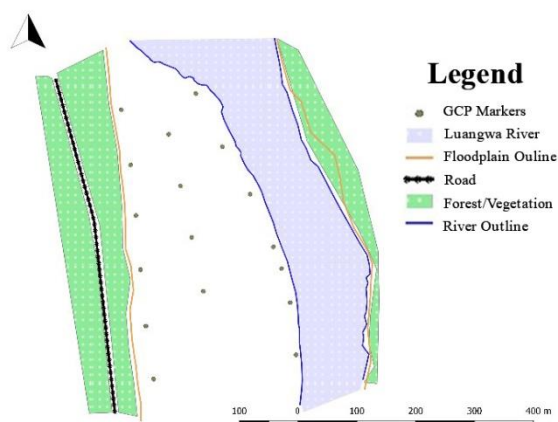


Figure 2 Location of GCPs on Floodplain

The UAV flew along 2 different paths at heights of 90m and 100 m respectively. The UAV camera was tilted at an angle of
165 10 degrees forward. The flight control application Pix4d Capture was used for its ability to adjust the camera angle. A total of
530 images were collected with a front and side overlap of 80% and 72% respectively.

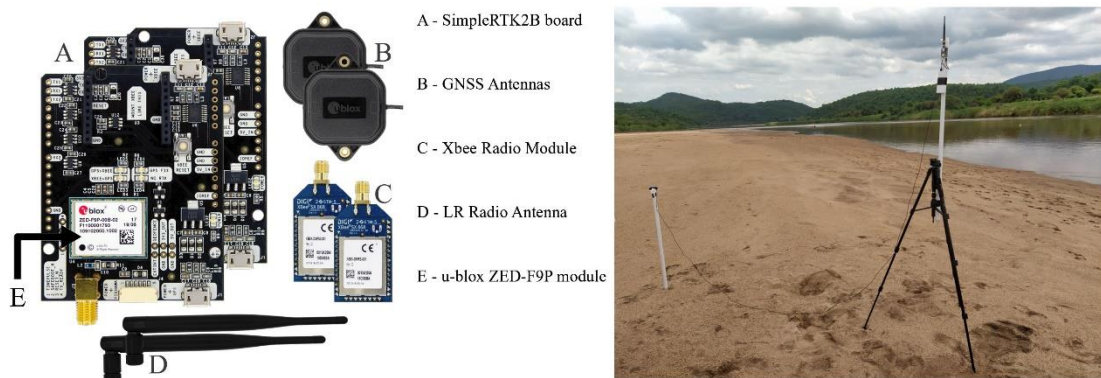


Figure 3 (a) RTK GNSS Equipment, 3 (b) Base setup on site

2.2.3 Wet River bathymetry

170 The Luangwa River, similar to other large tributary rivers of the Zambezi, is perennial meaning the bathymetry of the river
needs to be measured under flow conditions. The wet river bathymetry was recorded using a combination of an ADCP and
RTK GPS. The GPS of the ADCP was not used in favour of the RTK GPS for improved accuracy. The RTK GPS was mounted
directly onto the ADCP sonar beam, whilst the ADCP was attached to a canoe rowed by local fishermen, as shown in *Figure*
4(b). The ADCP and the RTK GPS were configured to take measurements at one second intervals. The canoe moved from one
175 side to the other in a zigzag manner and tried as much as possible to reach the edges to both sides. The GPS crossed the river
21 times and a total of 3102 measurements were recorded. The program suitable for the particular ADCP, Winriver II, was
used for real-time data collection. For the purposes of interpolation, the canoe was manoeuvred along both sides of the river.
The river was however shallow, especially on the right bank, this means that it was not possible for the canoe to adequately
move close to the water line. To compensate for this limitation, the RTK GPS was mounted on a wooden cart and towed
180 manually along the waterline. An image of the cart is shown in *Figure 4(a)*. The waterline track was subsequently used as the
true value reference to enable establishment of the level of deviation of the ODM and Agisoft values.



Figure 4(a) RTK GNSS mounted on a mobile cart, 4(b) ADCP attached to a fisherman's canoe

2.2.4 Processing the Dry and Wet Bathymetry

185 Images taken by the UAV are collected and fed into the ODM and Agisoft software. The images were processed locally on a Dell Core i7 8th generation machine with 32 Gigabytes of RAM. The same settings were applied in the processing steps as far as was permissible. *Figure 5 (b)* outlines the steps which were taken in the production of the point cloud and DEM.

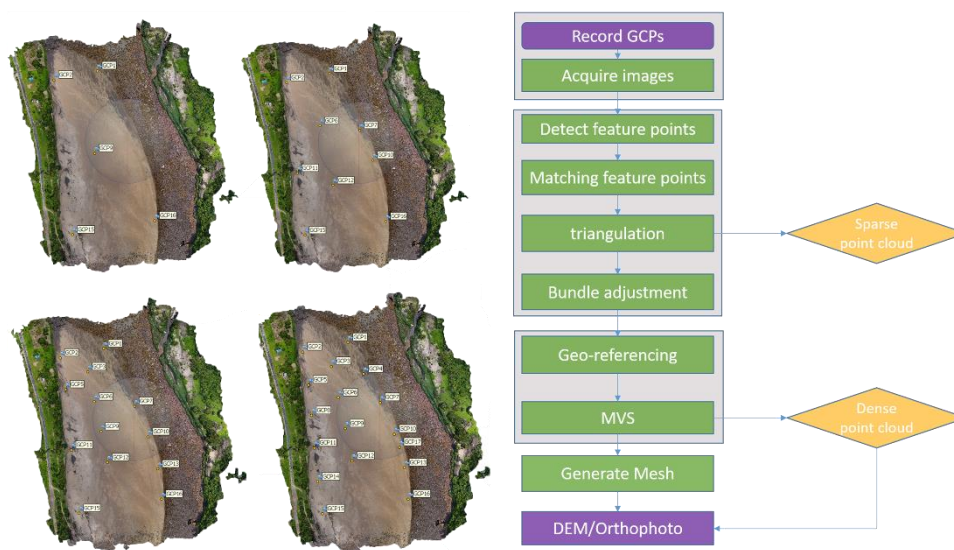


Figure 5(a) GCP Distribution Combinations [5, 9, 13, & 17], 5(b) Photogrammetry Process adapted from Balogh and Kiss (2014)

190 This process was repeated four times with different GCPs each time (5, 9, 13, 17 GCPs) for both software packages. The exact same GCPs were used for the reconstruction in both Agisoft ODM. *Figure 5 (a)* shows the locations and particular markers which were selected.

In order to combine the dry and wet bathymetry, point clouds of both extractions were processed in Cloud Compare software. The wet river bathymetry point cloud is processed as follows. Each measurement point taken on the river consists of the



195 attributes depth (measured with the ADCP), latitude, longitude and height (measured with the RTK GNSS). The depth
measurement is subtracted from the water height and combined with the longitudinal and latitudinal coordinates. Thereafter,
the point cloud is volumised without the RTK waterline, left bank and right bank tracks. The three tracks were then added and
subsequently volumized into a digital terrain model. When both point clouds (dry and wet bathymetry) are constructed
accordingly they are merged. To make sure that the resulting grid is seamless, another linear interpolation with the nearest non
200 empty cell (2.5D volume) is computed.

2.3 Reconstruction Experiments

2.3.1 Impact of the used processing software

A relatively simple experiment to judge if ODM can be used as a viable alternative to costly proprietary software was
employed. The experiment sought to validate the accuracy of open-source software versus commercially available software
205 by comparing ODM (open-source) with Agisoft Metashape (commercial), respectively. The availability of GCPs made this
possible. We considered the root mean square error (RMSE) of checkpoints. RMSE metric is widely employed as a measure
of conformity between two DEMs (Alidoost and Arefi, 2017). If the RMSE values are of comparable nature, comparing one
package against the other (magnitude, distribution, presence of outliers) then they perform similarly. To calculate these RMSE
values, only those reference points which were not used in the reconstruction were made use of, this allowed for an independent
210 estimation made by both software packages. The RMSE was computed using *Equation 2 and Equation 3* in the horizontal and
vertical direction respectively.

$$RMSE_{xy} = \sqrt{\frac{1}{n} \sum_{i=1}^n (\Delta X_i^2 + \Delta Y_i^2)} \quad (2)$$

$$RMSE_z = \sqrt{\frac{1}{n} \sum_{i=1}^n (\Delta Z_i^2)} \quad (3)$$

Where ΔX_i = residual of the i^{th} value in the x axis

ΔY_i = residual of the i^{th} value in the y axis

ΔZ_i = residual of the i^{th} value in the z axis

215 n = number of check points (GCPs that were not used in the reconstruction)

DEMs based on five, nine, thirteen and seventeen GCPs were exported from ODM and Agisoft. The DEMs were fed into the
Geographic Information System (GIS) QGIS and a point sampling tool was used to extract elevation values at the
corresponding coordinates of the GCPs that were not used in the reconstruction. This ensured that an independent estimate of
the RMSE could be established. A bootstrapping experiment was conducted on the errors of the individual GCPs that were
220 used to calculate the RMSE. This experiment was performed to test the stability of the RMSE. In the experiment random
samples of error were drawn from the 5, 9 and 13 GCPs. The sampled errors, which were equal in number to the available



GCPs, were sampled with replacement to obtain new RMSE values. The process was then repeated for 1000 drawn sample sets. Given that this first experiment led to the conclusion that ODM is a satisfactory choice and it is free and Open-Source (see Section 3.1) the remaining experiments were only conducted with ODM.

225 2.3.2 Impact of GCP placement and density on accuracy

This experimental objective was divided into two parts. The first was to establish the impact of GCP density on DEM accuracy. The second part was to establish the impact of placing GCPs further or closer to the flowing river. In both instances a comparison of absolute error was made with the RTK track line which was acquired using the RTK GNSS mounted on a mobile cart. The Python package ‘rasterio’ was used to extract elevation values at corresponding coordinates. For the first part, elevations from the DEMs with 5, 9 13 and 17 GCPs were extracted and compared to the RTK line elevations. For the second part, many studies have indicated that photogrammetry is incapable of adequately mapping a flowing river because it reflects light (Bandini et al., 2017; Dai et al., 2018). The noise generated on the river surface has a negative impact on the overall accuracy of the DEM. In order to establish the significance of this noise, elevation extrapolations from the DEMs constructed using 9 GCPs closest to the river and 9 GCPs furthest from the river were compared. *Figure 6* shows the positions of the GCPs placed further and closer to the river. The figure also shows an orthophoto to be able to identify the river’s water surface and other features such as the vegetation on the natural levee of the river’s floodplain.

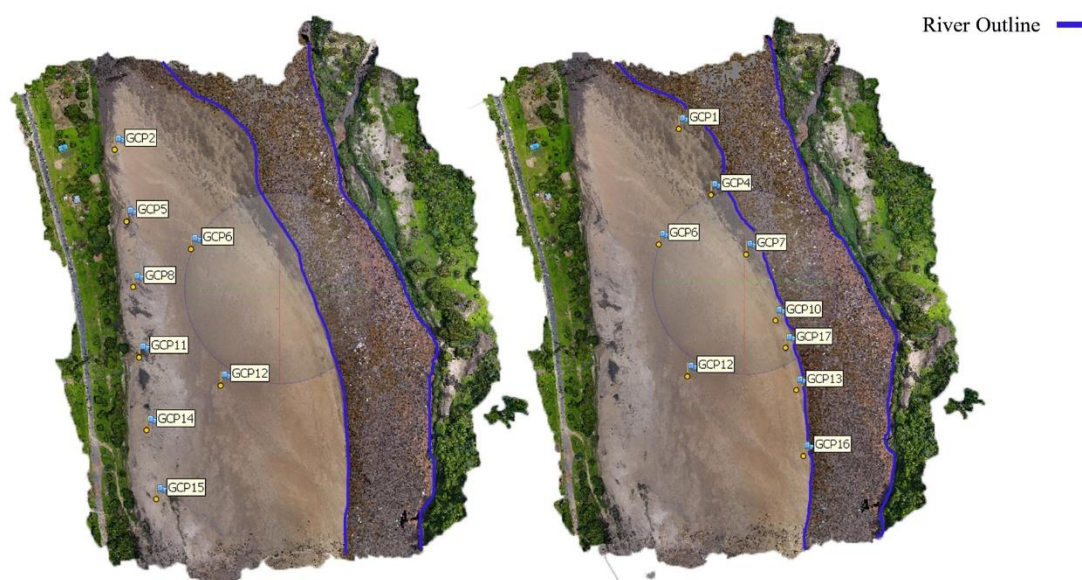


Figure 6 GCP distribution and river wetted perimeter during the survey, projected on an orthophoto result



2.3.3 Impact of DEM variations on hydraulic conveyance

240 We investigated how variations in DEM reconstruction choices impact on conveyance characteristics. We determined
conveyance versus depth relationships over several cross-sections in each DEM created. In addition, we compared DEM
derived hydraulic slope with an independent estimate of slope using an in-situ RTK GNSS tie line (see Section 2.2.3 for a
description of the acquisition method).

In order to obtain the full bathymetry of the river, the dry bathymetry and the wet bathymetry are merged together in the
245 software. Before the wet bathymetry is merged to the dry bathymetry, the wet river transects have to be volumised. This process
entails conversion of the sparse point cloud made of transect points into pixels through linear interpolation with the nearest
non-empty cell. In occurrences whereby there are overlaps or edges we choose to treat these through linear interpolation as
well. After merging, three cross sections perpendicular to the river were extracted such that a relationship between area and
perimeter could be established over the entire cross-section, including both wet and dry bathymetry. This was done for all the
250 elevation models generated using a different number of GCPs so that the established relationships could be compared. *Figure*
7 shows the location of the cross sections which were extracted from the respective reconstructions.

Slope estimation was conducted using two different techniques. The first involves the extraction of the slope from the terrain
outputs produced by the photogrammetry process. The second method calculated slope based on the entirely independent
reference track measured with the RTK GNSS on the cart. The outputs were then compared taking the slope derived by the
255 GNSS as the true value.

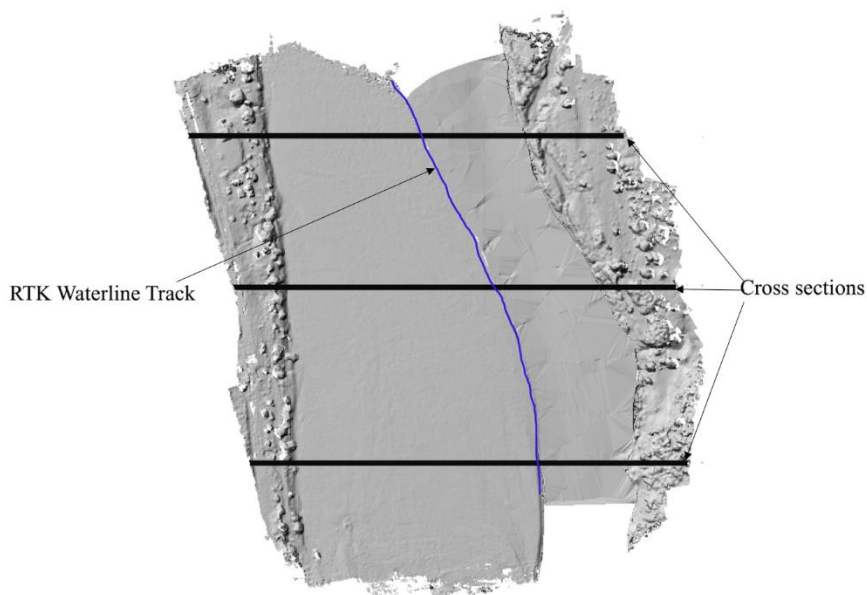


Figure 7 Cross section locations

3 Results

In summary, the assessment of the impact of processing methods on quality of terrain data, focussing on geometry of hydraulic properties consisted of three steps: applicability of open source versus proprietary photogrammetry software, the impact of GCP density and placement on DEM quality and the impact of variations in DEMs of flow estimation. In this section, we present the results of these three steps.

3.1 Impact of the used processing software

In order to assess the applicability of open source software the RMSE of terrain models processed in ODM were compared with those from Agisoft Metashape. The results are presented in *Table 1*.

Table 1 RMSE of different GCP combinations

	Agisoft		ODM (m)	
Configuration	Horizontal RMSE [m]	Vertical RMSE [m]	Horizontal RMSE [m]	Vertical RMSE [m]



5 GCPs	0.415	0.594	0.686	0.592
9 GCPs	0.259	0.290	0.406	0.344
13 GCPs	0.300	0.395	0.431	0.380

The results indicate Agisoft RMSE values that are comparable to those calculated when ODM was used for reconstruction. The two software products generally follow a trend whereby increasing the number of GCPs from 5 to 9 results in a notable decrease in RMSE. A further increase from 9 to 13 GCPs results in an increase in RMSE. This result is counter intuitive, however, given that the error was calculated based on GCPs which were not used in the reconstruction, it follows that increasing the number of GCPs simultaneously decreased the sample size available for error calculation. A reduced sample size meant that outlier error values may well result in a poorer resultant RMSE. In general, the RMSE values of Agisoft and ODM were similar, however, we note that the sample size of data used to calculate the RMSE was not large enough to provide statistical confidence. To that end, a bootstrapping experiment was conducted to establish if there was a significant similarity in the performance of ODM in comparison to Agisoft (see Section 2.3.1). The bootstrapping experiment is particularly appropriate for small sample sizes and data sets which do not necessarily follow a normal distribution (Freedman, 2007). The results of the bootstrap experiment are presented in *Figure 8*.

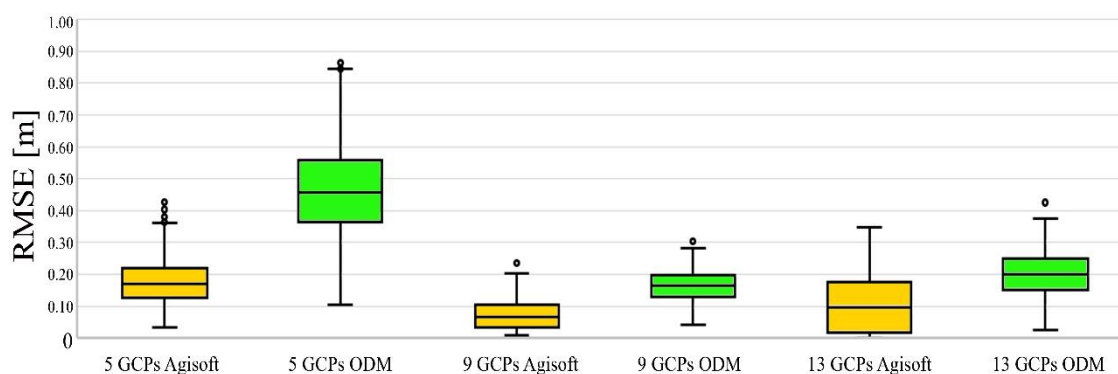


Figure 8 Bootstrap Box plot

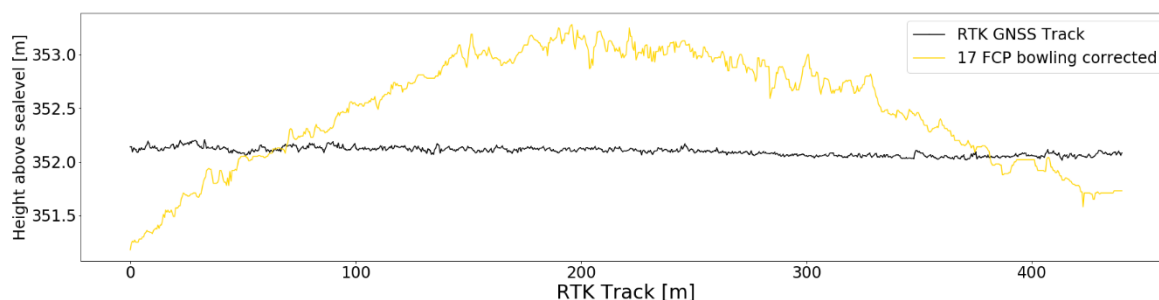
Using 5 GCPs, there is a relatively large difference between the RMSE of Agisoft and ODM. We attribute this difference to the inherent capacity of Agisoft to perform better than ODM in instances where there are few control points. The graph suggests that, out of the selected number of comparisons, 9 GCPs is the optimal balance between GCPs which correct the reconstruction



and a checkpoints to calculate the RMSE. The representation indicates a strong resemblance between errors in ODM and Agisoft. The results confirm the potential application of open-source software as an alternative for commercial options without significant compromise on accuracy. Accordingly, the remainder of the results are processed and analysed based on the ODM software package.

3.2 Impact of GCP placement and density on accuracy of hydraulic features

The aim of this experiment was to assess the impact of variations in the number of Ground Control Points (GCPs) and the distribution of the GCP markers on the quality of DEMs, with a particular emphasis on characteristics that impact on hydraulics. Five different GCP numbers (0, 5, 9, 13, and 17) and two specialised settings (Brown-Conrady and Fixed camera parameter) were compared. We observed dome-like deformations in all of the elevation extractions. This phenomenon, known as the ‘doming effect’ (also known as "bowling effect", described in section 2.2) is exemplified in *Figure 9*. The effect is apparent despite attempts to avoid the aforementioned phenomena through deliberate flight practices such as a 10° camera angle and a 20° alternating flight path.

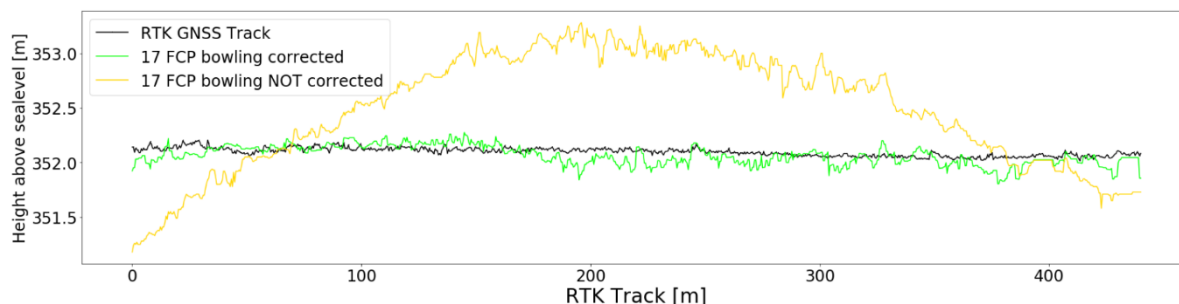


295

Figure 9 Doming effect

A rather practical approach was used to correct for the doming effect. A first order polynomial was fitted through the RTK GNSS track. A second order polynomial was then fitted through all the reconstructed point clouds. The error was then determined by calculating the absolute difference between the two polynomials for the given length. The respective clouds were divided into 1500 sections from north to south whereby every point within each section was assumed to be deformed by the same elevation value. The absolute errors were then applied as corrections to the point clouds depending on which section each location fell in. *Figure 10* shows corrections made to the reconstruction based on 5 GCPs. Appendix B shows the corrections which were performed on all other terrain clouds.

300



305 **Figure 10 Correction of the doming effect**

The assessment was conducted based on the RTK waterline track and the results are presented in *table 2*. The results indicate a decrease in the RMSE as we increase the number of GCPs. However the incremental benefit of increasing the number of GCPs beyond 5 becomes smaller as more control points were added to the reconstruction. Noticeably, the RMSEs derived based on the GCP checkpoints was similar to that which was obtained based on the RTK waterline as a reference. This implies that the RTK waterline track is a potential substitute when calculating the error in a photogrammetry reconstructed model. The RMSE values derived from the ‘No GCPs’ and from using the ‘Brown-Conrady’ configuration showed significant inaccuracy and therefore rendered inapplicable. However, the ‘Fixed Camera Parameter’ configuration performed reasonably well (RMSE = 0.618m), considering no control points were used.

Table 2 RMSE of different GCP combination and configurations

Configuration	RMSE _z [m] Based on RTK track
5 GCPs	0.558
9 GCPs	0.581
13 GCPs	0.486
17 GCPs	0.479
FCP	0.618

315 We identified a bias in terms of the errors calculated when GCPs are closer to or further from the river. The results are presented in *table 3*. Similar to the aforementioned experiment, the RTK track was used as a reference. The RMSE is less when GCPs closer to the river (approximately 20 m away) are used in the reconstruction than when GCPs further away are used. We hypothesize that the GCP distribution used in the experiment ‘Closer to River’, is such that GCPs are placed much closer to



the reference line, therefore better conditioning the part of the reconstruction close to the RTK track. Our hypothesis is
320 reaffirmed by the results of calculating the RMSE based on GCPs as shown in table 3. Similarly, the RMSE is less when GCPs
used in the reconstruction are closer to the River.

Table 3 RMSE comparison further and closer to the river

Configuration	ODM RMSE error	
	RMSE [m] Based on RTK line	RMSE [m] Based on GCPs
Closer to River	0.374	0.242
Further from River	0.771	0.926

3.3 Impact of DEM variations on hydraulic conveyance

Hydraulic conveyance was computed from the merged dry and wet bathymetry. We performed a comparison of the hydraulic
325 conveyance across various reconstructions. Furthermore, we compared the hydraulic slope of the various reconstructions with
an independent slope estimate measured from an in-situ RTK GNSS tie line. In order to extract the cross-section elevations,
the full bathymetry of the river had to be utilised. The wet river point cloud, shown in *Figure 11*, covers 555 metres of the
river length and consists of 5,164 points. The latitude and longitude originate from RTK GPS measurements whereas the height
component is determined using both RTK GNSS and an ADCP as described in section 2.2. The maximum and minimum
330 height of the point cloud are 352.20 and 348.45 metres respectively.

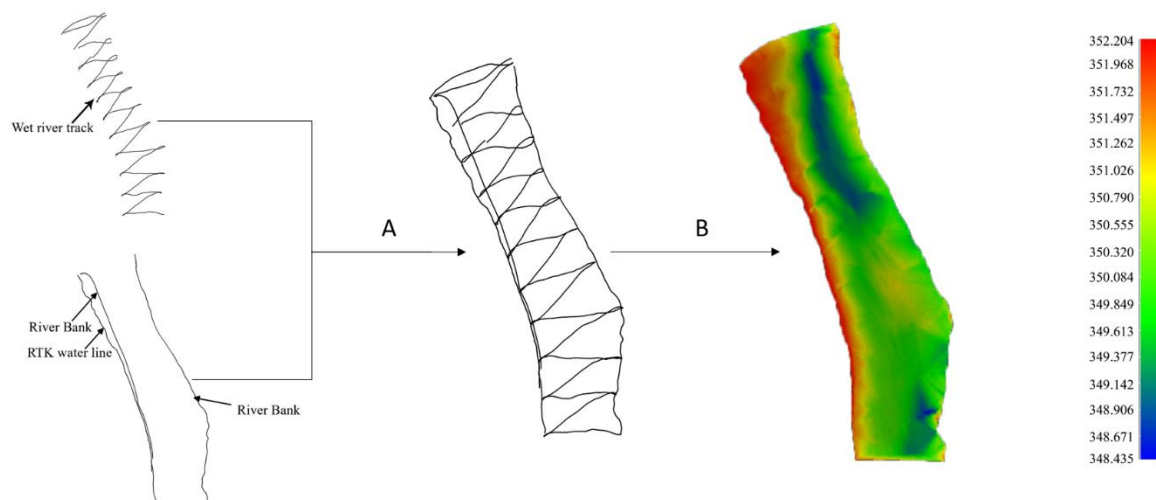


Figure 11 Wet Bathymetry processing (A-Merging B- Volumisation)

The dry river bathymetry is constructed using photogrammetry and RTK GNSS as described in section 2.2. The various point clouds represent an area of approximately 679 x 551 metres. Like the wet river, each point contains a latitude, longitude and height component with a maximum and minimum height of 383.4 (hill in the south east corner) and 350.2 metres respectively.

In order to extract the cross-sections, the dry and wet bathymetry had to be merged and subsequently volumised. These two processes which were conducted in Cloud Compare are exemplified in *Figure 12*.

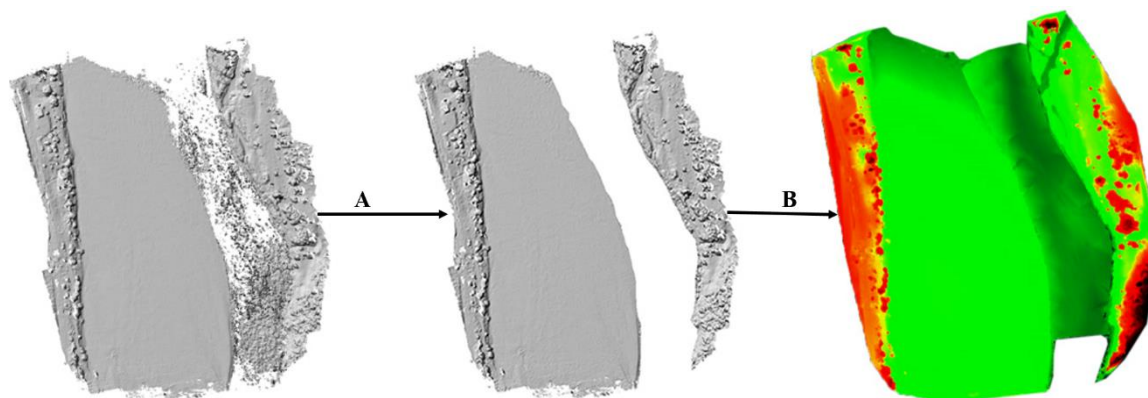


Figure 12 Floodplain processing (A-extraction of water surface, B-Merging with wet bathymetry and volumising Volumisation).



Figure 13 shows an extraction of the cross section on the northern side of the terrain model. The GCP configuration with 5, 9, 13 and 17 GCPs present very similar cross-sectional properties. The results are similar for all cross sections (Appendix B4). The configuration with no GCPs and Brown-Conrady significantly underestimated the actual height by approximately 13 meters.

345 In an attempt to improve the results when no GCPs are available, we applied a configuration setting known as FCP (Fixed Camera Parameters). The FCP turns off camera optimisation while performing bundle adjustment. Bundle adjustment is a technique for calculating the errors that occur when we transform the XYZ location of a point in the environment to a pixel point on a camera image. In certain circumstances, particularly when mapping linear (low amplitude, limited features) topographies such as the Luangwa floodplain, bundle adjustment performs poor estimation of distortion parameters (Griffiths and Burningham, 2019).
350 The FCP results showed a significant improvement, the shape of the cross section was similar to the experiments with GCPs though visibly below the rest.

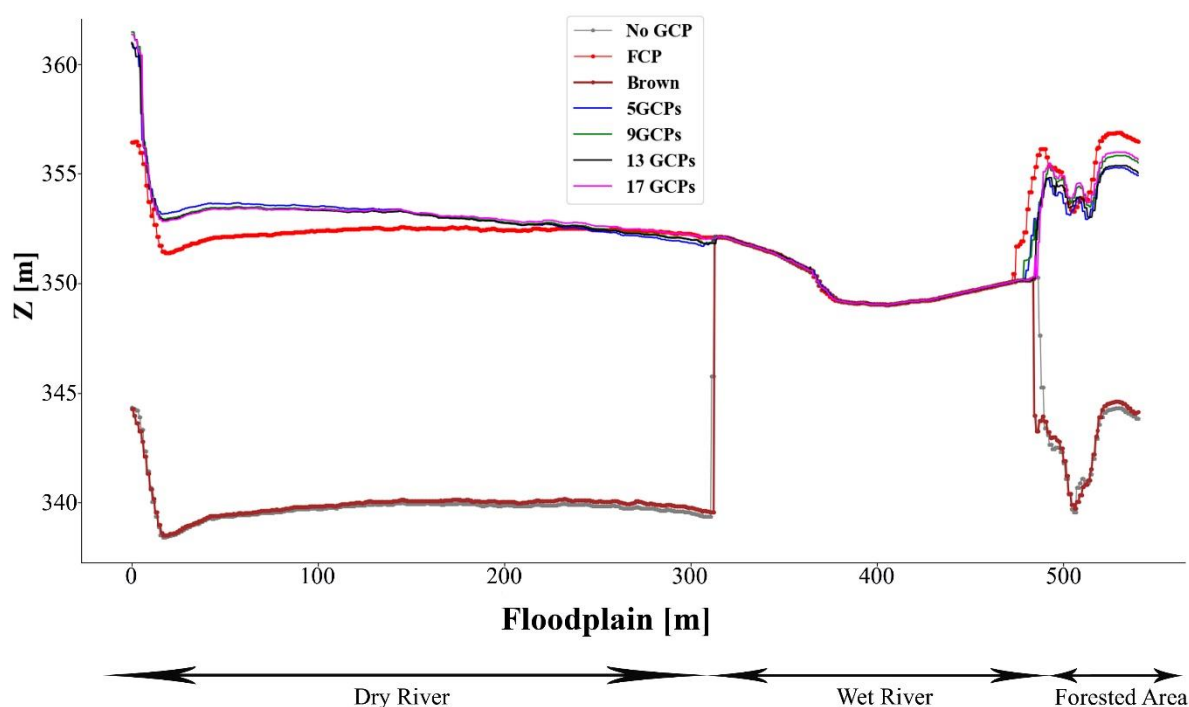
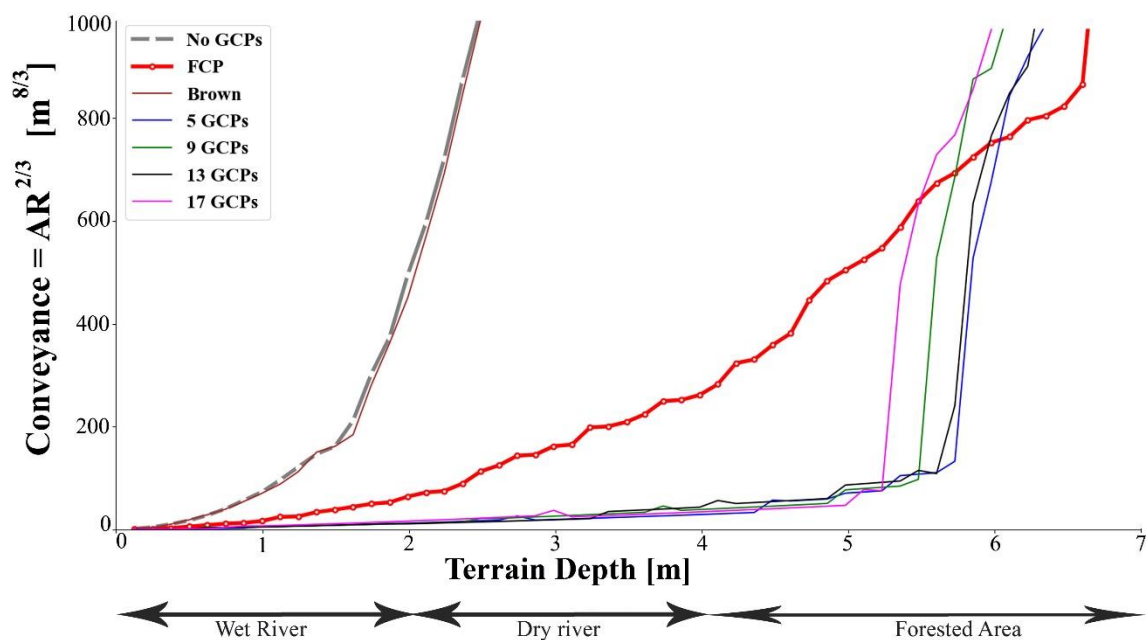


Figure 13 Cross section 1 extract

The hydraulic conveyance estimation graph is presented in Figure 14. As anticipated, results indicate no significant difference among conveyances estimated based on 5, 9, 13, and 17 GCPs. The conveyances estimated based on the 'no GCP' and 'Brown-Conrady' configuration are not meaningful because of the clear offset between the photogrammetry results and the RTK results. The conveyance based on the FCP performed better than Brown Conrady and no GCP configuration. However, the



estimated conveyance was significantly different from the conveyances estimated using GCPs. The results were similar for all 3 cross sections (Appendix B)



360

Figure 14 Cross section 1 (south of the terrain) conveyance vs depth relationship

The slope calculations shown *table 4* a significant difference between the true slope (RTK GNSS), and the photogrammetry derived slope values. This is despite a correction of the doming effect as described in *section 3.2*. Among photogrammetry based slope derivations, there were relatively large variations

365 **Table 4** Slope estimations

Configuration	Hydraulic slope [* 10 ⁻⁴ m]
RTK GNSS Track	-2.300
5 GCPs	-3.935



9 GCPs	-3.286
13 GCPs	-3.749
17 GCPs	-3.891
No GCPs FCP	-3.995

4 Conclusions and Recommendations

This study reinforced the capability of low-cost instruments, such as UAVs in combination with RTK GNSS, being applied to perform physically based remote river rating. The performance of the open-source photogrammetry software substantiated the claim that, free and open-source available packages, are capable of producing results which are as good as proprietary alternatives as shown by the RMSE analyses. Across different GCP distributions, no significant difference was observed between the errors calculated based on open-source software and those calculated based on commercial software packages. This, combined with the fact that a UAV can be acquired relatively and would be affordable to many water management institutions in low income economies opens doors for use in low resource settings. Apart from cost implications, the open-source software provided an option in the form of a ‘fixed camera parameter’ configuration which significantly reduced the RMSE of the reconstruction, even without the use of GCPs. The results had limitations in terms of the sample size used for calculating the RMSE of the GCPs. For instance, when reconstruction was performed based on 13 GCPs, only 4 GCPs were available to use as validation points. In future studies, it would also be useful not only increase the number of independent checkpoints but to also measure the RTK track further away from the river to avoid influence of poor river photogrammetry reconstruction.

As anticipated, increasing the number of GCPs had an inverse effect on the RMSE. However, the gradual improvement in accuracy of the reconstruction diminished disproportionately. For the selected trials, a reconstruction based on 9 GCPs provides the most accurate RMSE results. It provides an optimal balance between the number of GCPs for reconstruction and the number of validation points. In addition, we note that accuracy cannot be determined based on GCP density alone. The distribution of GCPs proves to be as critical as the GCP density in order to achieve optimal accuracy. In certain cases, priority must be placed on the GCP distribution so that the output is representative of a wider range of elevation values. Placing more



GCPs in proximity to potentially problematic areas such as forests or water significantly improves the overall output of the reconstruction.

390 The effective impact of variations in GCPs on geometry is realised in the form of conveyance. Despite the optimal number of
GCPs being nine (9), the study concludes that five (5) GCPs evenly spread out across a floodplain of approximately 40 hectares
and flying at an elevation of 100 m is sufficient to generate an elevation model that meets the requirements of accurate
conveyance estimation. Configurations such as the FCP, advance the model reconstruction but do not achieve satisfactory
accuracy without GCPs. Slope estimation based on photogrammetry reconstructions was not satisfactory under any GCP
395 configuration tested. The novel method of measuring an RTK GNSS line is therefore a critical alternative to establish the slope
by correcting for the doming effect.

A novel approach to generate a seamless bathymetry through merging and volumisation was successfully tested. Results
presented here encourage future studies to investigate the impact of variations in the number of GCPs on discharge estimations
in a hydraulic model with different hydrodynamic boundary conditions. Within the envisioned hydraulic model it would be
important to extend terrain downward to reduce backwater effects.

400



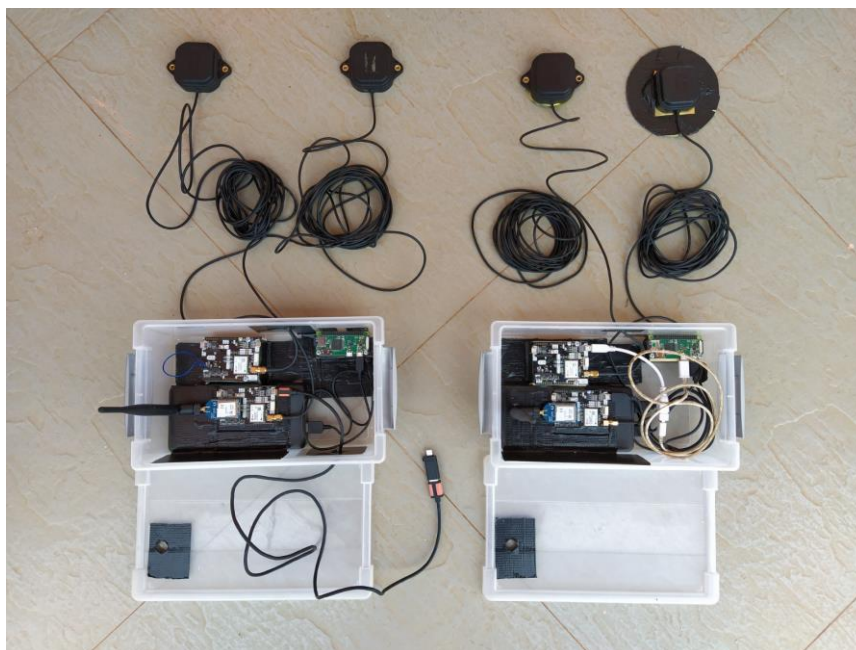
405

A

Data Collection

This appendix contains figures, tables and photo which complement the data collection method.

Figure A.1 shows the components and setup of the constructed Real Time Kinematic GNSS. The container on the right-hand side in Figure A.1 contains the base, the other container contains the rover. Both containers include two SimpleRTK2B boards with a u-blox-ZED9P module, a Raspberry Pi, two GNSS antennas, an XBEE shield and a long range radio antenna. With this hardware, two complete RTK GNSS sets can be constructed, one based on long range radio communication and one based on a 4G internet connection. The SimpleRTK2B board with the XBEE shield works with the radio module and is used during the fieldwork.



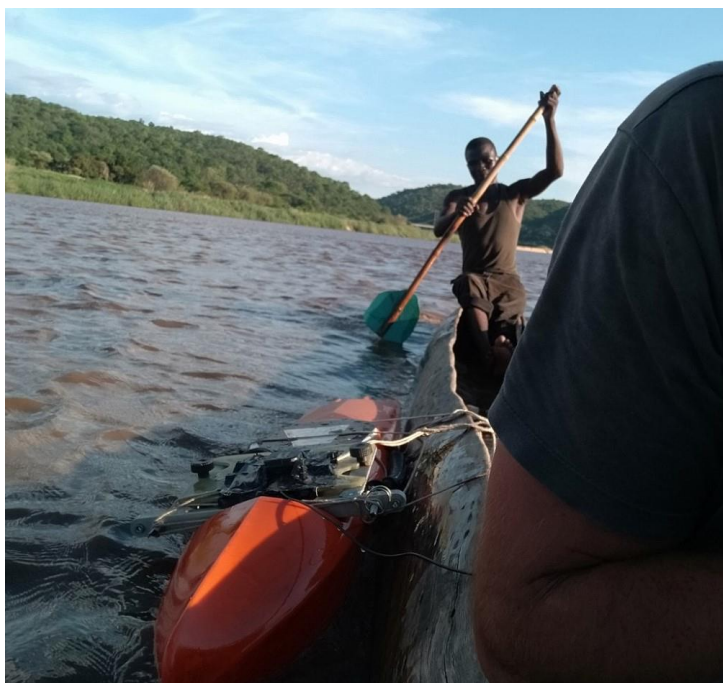
415

A 1 RTK GNSS Equipment

Figure B.1 shows the bathymetric data collection setup with the ADCP tied to the wooden canoe of a local boatman. On top of the sonar an RTK GNSS receiver is mounted which is, via a SimpleRTK2B board, connected to a smartphone logging the



420 location measurements with a one second time interval. The ADCP is connected to a laptop running Winriver II which stores
the depth measurements. Figure B.1: The ADCP connected to the canoe with the GNSS receiver mounted on top of the sonar.



A 2 ADCP attached to canoe

425

430

435



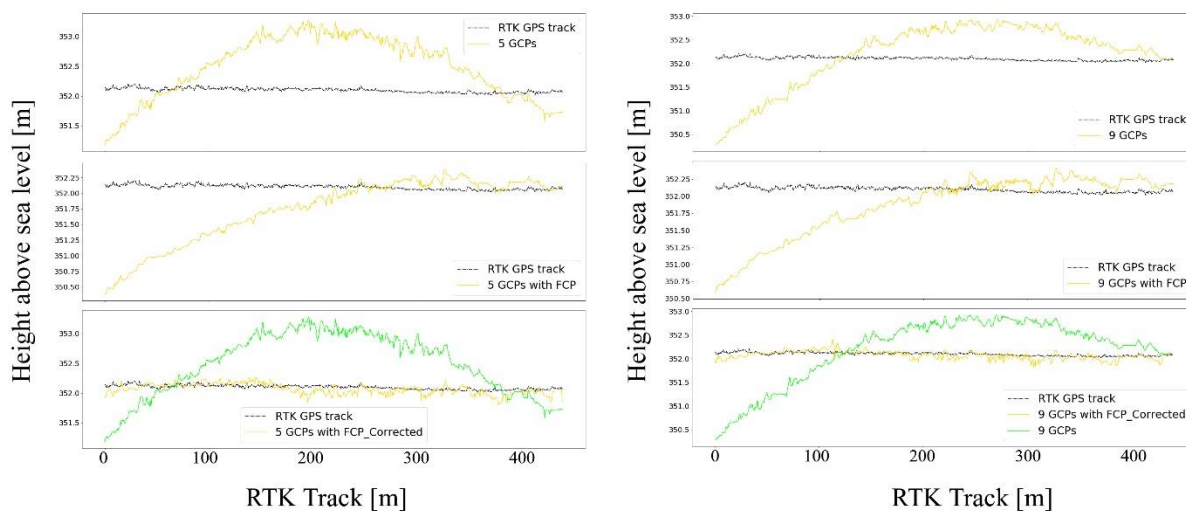
440

B

Wet and Dry Bathymetry

445 *Figure B1* shows the ‘bowling’ or ‘doming’ effect on terrain models. The top left graph represents the relationship between height and track for the 5 GCP terrain. The centre left graph represents the relationship between and track for the 5 GCP terrain after FCP correction. The bottom left graph represents the relationship between and track for the 5 GCP terrain after both FCP and doming correction. The top right graph represents the relationship between height and track for the 9 GCP terrain. The centre right graph represents the relationship between and track for the 9 GCP terrain after FCP correction. The bottom right graph represents the relationship between and track for the 9 GCP terrain after both FCP and doming correction.

450



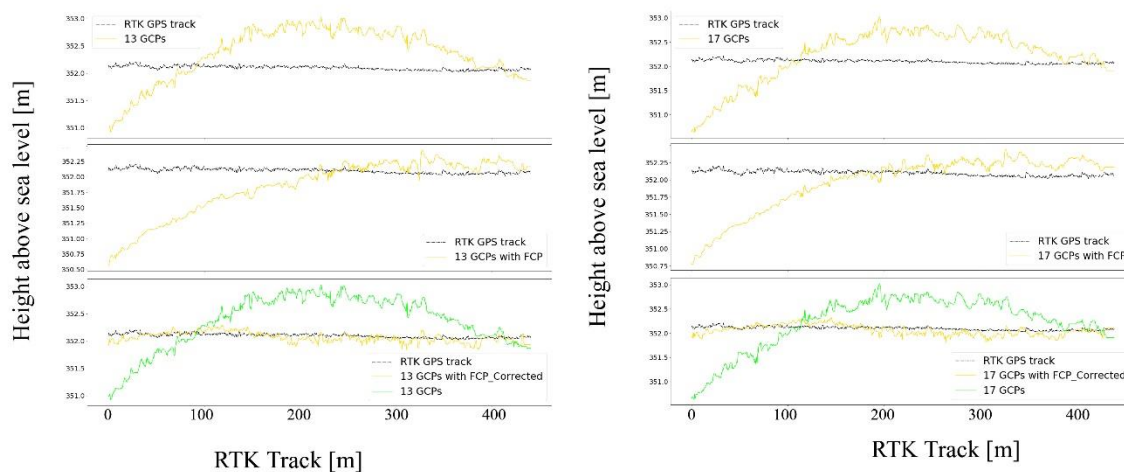
B 1 Correction for the doming effect

Figure B2 shows the ‘bowling’ or ‘doming’ doming effect on terrain models. The top left graph represents the relationship between height and track for the 13 GCP terrain. The centre left graph represents the relationship between and track for the 13

455



GCP terrain after FCP correction. The bottom left graph represents the relationship between and track for the 13 GCP terrain after both FCP and doming correction. The top right graph represents the relationship between height and track for the 17 GCP terrain. The centre right graph represents the relationship between and track for the 17 GCP terrain after FCP correction. The bottom right graph represents the relationship between and track for the 17 GCP terrain after both FCP and doming correction.

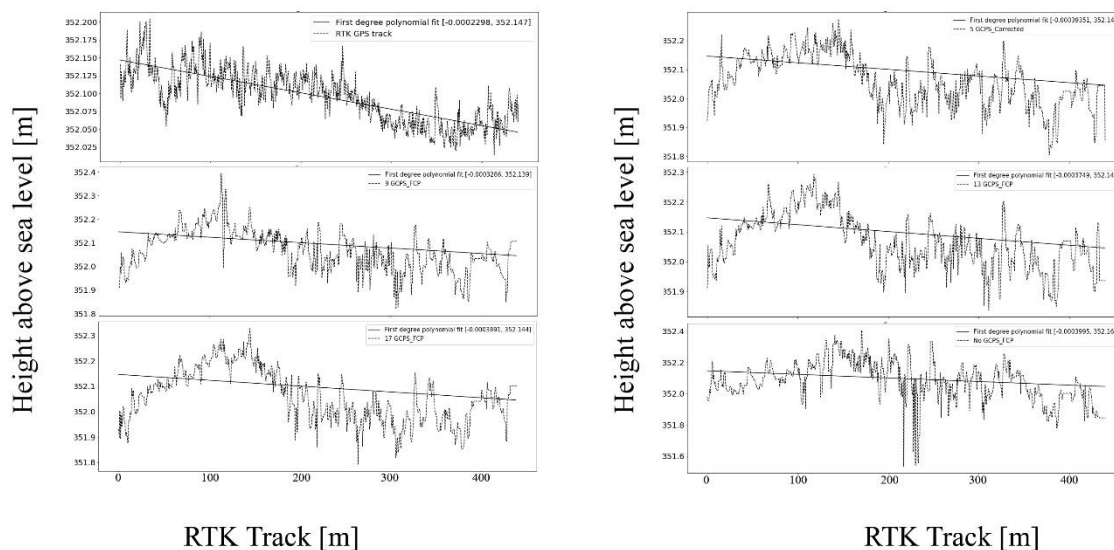


460

B 2 Correcting the doming effect

Figure B3 shows the regression line fit through extracted tracks lines. The top left graph represents the relationship between height and track for the RTK track. The centre left graph represents the relationship between height and track for the 9 GCP. The bottom left graph represents the relationship between height and track for the 17 GCP terrain. The top right graph represents the relationship between height and track for the 5 GCP terrain. The centre right graph represents the relationship between height and track for the 13 GCP. The bottom right graph represents the relationship between height and track for the no GCP terrain

465

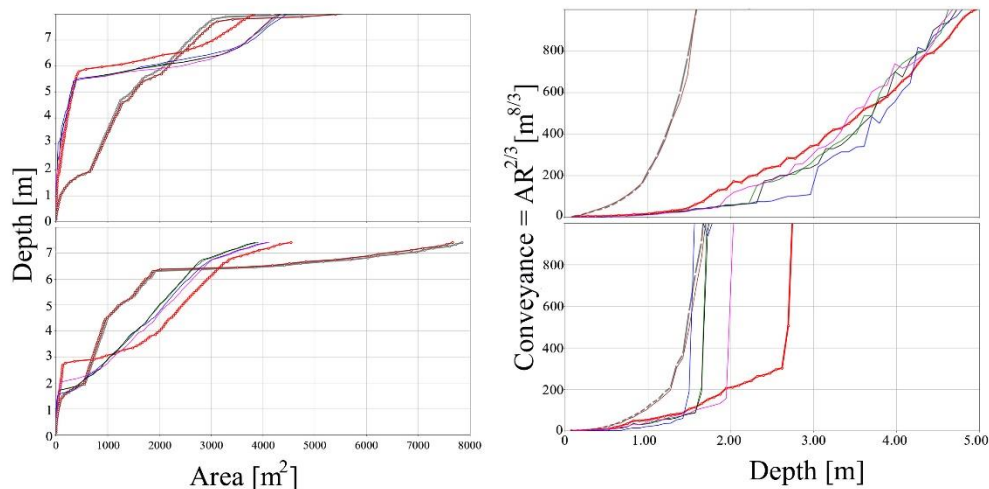


RTK Track [m]

RTK Track [m]

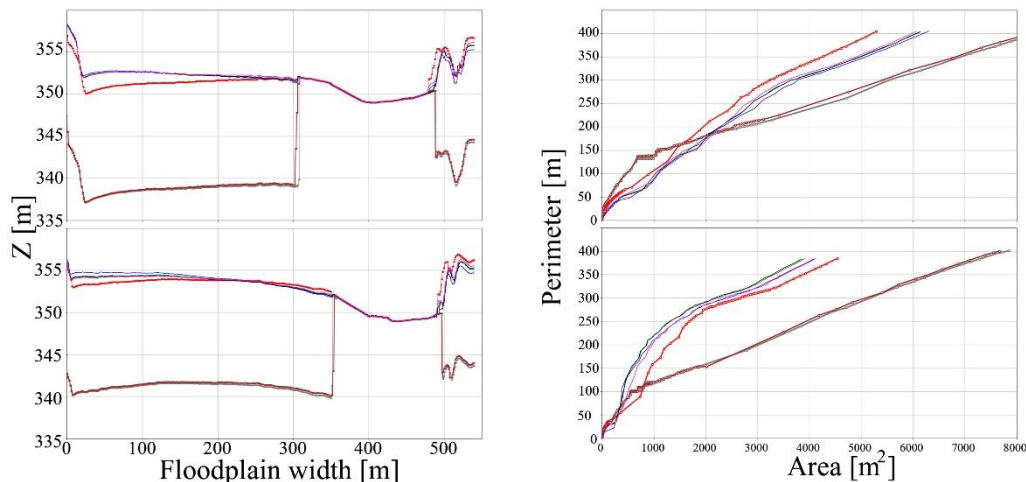
470 **B 3 First order polynomials through extracted tracks**

Figure B4 shows the relationship between depth and area, as well as the relationship between depth and conveyance. The top left graph represents the relationship between depth and area at the cross section on the northern part of the terrain. The top right graph represents the relationship between depth and conveyance at the cross section on the northern part of the terrain. 475 The bottom left graph represents the relationship between depth and area at the cross section on the northern part of the terrain. The bottom right graph represents the relationship between depth and conveyance at the cross section on the northern part of the terrain.



B 4 Depth vs Area Map and Conveyance vs Depth

480 Figure B5 shows the relationships between floodplain width and height above mean sea level, as well as the relationships between wetted perimeter and area. The top left graph represents the relationship between floodplain width and height above mean sea level at the cross section on the northern part of the terrain. The top right graph represents the relationship between wetted perimeter and area at the cross section on the northern part of the terrain. The bottom left graph represents the relationship between floodplain width and height above mean sea level at the cross section on the northern part of the terrain. The bottom right graph represents the relationship between wetted perimeter and area at the cross section on the northern part of the terrain.



B 5 Height vs width graph and Perimeter vs Area



490 **Data Availability**

Images used to carry out the ODM photogrammetry can be found on <https://doi.org/10.4121/14865225>.

Author Contributions

Hubert Samboko performed conceptualisation, data curation, formal analysis, investigation and writing the original draft. Hessel Winsemius performed conceptualisation, reviewing, editing and supervision. Sten Schurer performed data curation and
495 investigation. Hodson Makurira performed supervision, reviewing and editing. Kawawa Banda performed reviewing and editing. Hubert Savenije performed funds acquisition, supervision, reviewing and editing.

Competing interests

The authors declare that they have no conflict of interest

500 **References**

- Alidoost, F. and Arefi, H.: Comparison of UAS-based photogrammetry software for 3d point cloud generation: a survey over a historical site, *ISPRS Ann. Photogramm. Remote Sens. Spat. Inf. Sci.*, 4(4W4), 55–61, doi:10.5194/isprs-annals-IV-4-W4-55-2017, 2017.
- Awasthi, B., Karki, S., Regmi, P., Singh Dhami, D., Thapa, S. and Panday, U. S.: Analyzing The Effect of Distribution Pattern
505 & Number of GCPs on Overall Accuracy of UAV Photogrammetry Results., 2019.
- Balogh, A. and Kiss, K. A.: Photogrammetric processing of aerial photographs aquired by UAVs, *Hungarian Archaeol.*, 40, 1–8. [online] Available from: https://www.academia.edu/7070293/Photogrammetric_processing_of_aerial_photographs_aquired_by_UAVs (Accessed 2 April 2019), 2014.
- 510 Bandini, F., Olesen, D., Jakobsen, J., Kittel, C. M. M., Wang, S., Garcia, M. and Bauer-Gottwein, P.: Bathymetry observations of inland water bodies using a tethered single-beam sonar controlled by an Unmanned Aerial Vehicle, *Hydrol. Earth Syst. Sci. Discuss.*, 1–23, doi:10.5194/hess-2017-625, 2017.
- Chow, V.: *Open-channel hydraulics.*, McGraw-Hill Book Company, New York., 1959.
- Colomina, I. and Molina, P.: Unmanned aerial systems for photogrammetry and remote sensing: A review, *ISPRS J. Photogramm. Remote Sens.*, 92, 79–97, doi:10.1016/J.ISPRSJPRS.2014.02.013, 2014.
- 515 Costa, J. E., Spicer, K. R., Cheng, R. T., Haeni, F. P., Melcher, N. B., Thurman, E. M., Plant, W. J. and Keller, W. C.: Measuring stream discharge by non-contact methods: A proof-of-concept experiment. [online] Available from:



- <http://citeserx.ist.psu.edu/viewdoc/download;jsessionid=402EFED54B1E25BD2513F8455430828D?doi=10.1.1.469.2760&rep=rep1&type=pdf> (Accessed 26 December 2018), 2000.
- 520 Coveney, S. and Roberts, K.: Lightweight UAV digital elevation models and orthoimagery for environmental applications: data accuracy evaluation and potential for river flood risk modelling, *Int. J. Remote Sens.*, 38(8–10), 3159–3180, doi:10.1080/01431161.2017.1292074, 2017.
- Dai, C., Durand, M., Howat, I. M., Altenau, E. H. and Pavelsky, T. M.: Estimating River Surface Elevation From ArcticDEM, *Geophys. Res. Lett.*, 45(7), 3107–3114, doi:10.1002/2018GL077379, 2018.
- 525 Feurer, D., Bailly, J.-S., Puech, C., Le Coarer, Y. and Viau, A.: Very-high-resolution mapping of river-immersed topography by remote sensing. [online] Available from: <https://hal.archives-ouvertes.fr/hal-00585200> (Accessed 20 April 2021), 2008.
- Freedman, D. A.: Bootstrapping Regression Models, *Ann. Stat.*, 9(6), 1218–1228, doi:10.1214/aos/1176345638, 2007.
- Gindraux, S., Boesch, R. and Farinotti, D.: Accuracy Assessment of Digital Surface Models from Unmanned Aerial Vehicles’ Imagery on Glaciers, *Remote Sens.*, 9(2), 186, doi:10.3390/rs9020186, 2017.
- 530 Griffiths, D. and Burningham, H.: Comparison of pre- and self-calibrated camera calibration models for UAS-derived nadir imagery for a SfM application, *Prog. Phys. Geogr.*, 43(2), 215–235, doi:10.1177/0309133318788964, 2019.
- Grussenmeyer, P. and Khalil, O.: (PDF) A comparison of photogrammetry software packages for the documentation of buildings, *Remote Sens. Spat. Inf. Sci.* [online] Available from: https://www.researchgate.net/publication/32227934_A_comparison_of_photogrammetry_software_packages_for_the_documentation_of_buildings (Accessed 15 October 2020), 2008.
- 535 Herschy, R. W.: Streamflow measurement, Routledge. [online] Available from: <https://epdf.tips/streamflow-measurement-third-edition.html> (Accessed 28 March 2019), 2009.
- James, M. R. and Robson, S.: Mitigating systematic error in topographic models derived from UAV and ground-based image networks, *Earth Surf. Process. Landforms*, 39(10), 1413–1420, doi:10.1002/esp.3609, 2014.
- 540 Magri, L. and Toldo, R.: Bending the doming effect in structure from motion reconstructions through bundle adjustment, in *International Archives of the Photogrammetry, Remote Sensing and Spatial Information Sciences - ISPRS Archives*, vol. 42, pp. 235–241, International Society for Photogrammetry and Remote Sensing., 2017.
- Mansanarez, V., Westerberg, I. K., Lam, N. and Lyon, S. W.: Rapid Stage-Discharge Rating Curve Assessment Using Hydraulic Modeling in an Uncertainty Framework, *Water Resour. Res.*, 55(11), 9765–9787, doi:10.1029/2018WR024176, 545 2019.
- Mazzoleni, M., Paron, P., Reali, A., Juizo, D., Manane, J. and Brandimarte, L.: Testing UAV-derived topography for hydraulic modelling in a tropical environment, *Nat. Hazards*, 103(1), 139–163, doi:10.1007/s11069-020-03963-4, 2020.
- Mosley, M. and McKerchar, A.: *Handbook of hydrology*. [online] Available from: http://dl.watereng.ir/HANDBOOK_OF_HYDROLOGY.PDF (Accessed 27 April 2021), 1993.
- 550 Petersen-Øverleir, A., Soot, A. and Reitan, T.: Bayesian rating curve inference as a streamflow data quality assessment tool, *Water Resour. Manag.*, 23(9), 1835–1842, doi:10.1007/s11269-008-9354-5, 2009.



- Probst, A., Gatzliolis, D. and Strigul, N.: Intercomparison of photogrammetry software for three-dimensional vegetation modelling, *R. Soc. open sci.*, doi:10.1098/rsos.172192, 2018.
- Rantz, S. E. and Others, A.: Measurement and Computation of Streamflow: Volume 1. Measurement of Stage and Discharge, 555 Vol. 1 - Meas. Stage Discharge, USGS Water Supply Pap. 2175, 1, 313, doi:10.1029/WR017i001p00131, 1982.
- Salamí, E., Barrado, C. and Pastor, E.: UAV Flight Experiments Applied to the Remote Sensing of Vegetated Areas, *Remote Sens.*, 6(11), 11051–11081, doi:10.3390/rs61111051, 2014.
- Samboko, H. T., Abasa, I., Luxemburg, W. M. J., Savenije, H. H. G., Makurira, H., Banda, K. and Winsemius, H. C.: Evaluation and improvement of Remote sensing-based methods for River flow Management, *Phys. Chem. Earth*, 2019.
- 560 WARMA: Luangwa Catchment., [online] Available from: <http://www.warma.org.zm/index.php/%0Acatchments/luangwa-catchment> (Accessed 4 September 2019), 2016.
- Yang, C., Everitt, J. H. and Bradford, J. M.: Comparison of QuickBird Satellite Imagery and Airborne Imagery for Mapping Grain Sorghum Yield Patterns, *Precis. Agric.*, 7, 2006.
- Zečević, Ž., Popović, T., Member, S. and Krstajić, B.: Cloud Based Solution for Automatic Image Mosaicking and 565 Georeferencing, , (May 2018), 2017.
- Zheng, X., Tarboton, D. G., Maidment, D. R., Liu, Y. Y. and Passalacqua, P.: River Channel Geometry and Rating Curve Estimation Using Height above the Nearest Drainage, *J. Am. Water Resour. Assoc.*, 54(4), 785–806, doi:10.1111/1752-1688.12661, 2018.

570

Acknowledgments

This work is part of the research programme ZAMSECUR with project number W 07.303.102, which is financed by the Netherlands Organisation for Scientific Research (NWO). This research received and continues to receive support from the 575 University of Zambia and the Zambian Water Resources Management Authority.